Prediction of Uncompensated Polarity in Ultrathin Films

Jacek Goniakowski,[1] Claudine Noguera,[1] and Livia Giordano[2]

[1]*Institut des Nanosciences de Paris, Universités Paris 6–7 and UMR CNRS 7588, 140, rue de Lourmel, 75015 Paris, France*
[2]*Dipartimento di Scienza dei Materiali, Università Milano-Bicocca, Istituto Nazionale per la Fisica della Materia, Milano, Italia*

(Received 6 November 2006; published 17 May 2007)

Relying on first principles simulations of stoichiometric MgO, ZnO, and NaCl (1×1) ultrathin (111) films, we demonstrate the existence of a critical thickness below which polarity is uncompensated: the surface charges are bulklike, and the total dipole moment and the formation energy grow linearly with thickness. This study reveals novel facets of the problematics of polarity akin to the nanoscopic size of the objects and opens stimulating perspectives on polar nanostructures with surface properties and reactivity unaffected by charge compensation as in macroscopic samples.

DOI: 10.1103/PhysRevLett.98.205701 PACS numbers: 64.70.Nd, 68.55.Jk, 81.30.Dz

Ionic crystals that consist of alternating layers of oppositely charged ions produce an accumulating dipole moment which diverges with increasing thickness. The associated electrostatic potential increases linearly and leads to an energetically highly unstable situation, as exemplified by the infinite cleavage energy predicted in an ionic model [1]. In practice, all polar configurations studied both theoretically and experimentally until now are in fact always compensated. This means that the electrostatic divergence is healed by the presence of additional (compensating) surface charges, which quench the macroscopic dipole, assure a finite surface energy, and thus stabilize the entire stacking [2]. Various microscopic mechanisms yielding these compensating charges have been proposed, among which massive nonstoichiometry (with or without a long range order), partial occupation of the surface band (metallic surface), and adsorption of metal atoms or of charged species [2].

The situation seems drastically different in the case of nanosize objects, such as ultrathin oxide films. Attempts to produce clean, stoichiometric, and unreconstructed (111) films of MnO [3], MgO [4], FeO [5], CoO [6], NaCl [7], or (0001) films of ZnO [8] suggest that there may exist some uncompensated configurations. This implies that polarity of nano-objects may exhibit a qualitatively different nature. Indeed, in a previous theoretical study [9], we have predicted that ultrathin films may avoid polarity through a sound structural transformation. As revealed by the structural phase diagram of MgO(111) films, Fig. 1, at small thickness, the nonpolar graphiticlike *h*-BN(0001) phase is by far more stable than any other structure derived from the rocksalt (RS) MgO(111) orientation, including the (2×2) octopole reconstruction, known to stabilize efficiently the MgO(111) surface [10]. A similar structural transformation based on a wurtzite to graphiticlike transition was later proposed for thin films of materials with bulk wurtzite structure [11].

Beyond these findings, in the present Letter we reveal the unusual and strongly size dependent properties of another low energy phase of the diagram, Fig. 1, namely, the fcc zinc blende (ZB) phase (both rocksalt and wurtzite phases being unstable at small thickness). Whereas somewhat less energetically favorable than the graphiticlike phase, at small thickness it may represent a likely alternative (metastable) configuration if one takes into account the kinetic limitations akin to epitaxial film preparation.

Contrary to hexagonal graphiticlike(0001), an fcc (111) stacking, corresponding to a distorted zinc blende structure, is intrinsically polar. We will show that, contrary to all macroscopic systems studied both experimentally and theoretically in the past, at low thickness its polarity is *uncompensated*. Indeed, relying on first principles simulations of stoichiometric (1×1) MgO, ZnO, and NaCl fcc (111) films, we demonstrate that, below a critical thickness, their properties are driven by the accumulation of dipole moments, a signature of uncompensated polarity. Although the latter is qualitatively different from the compensated one, well described in the literature, we will sketch a unified conceptual framework which accounts for the electronic and energetic characteristics of both low- and high-thickness regimes. In our opinion, the control of the dipole moment via the film thickness is a powerful tool towards a fine-tuning of their properties, e.g., reactivity [12], or wetting ability [13].

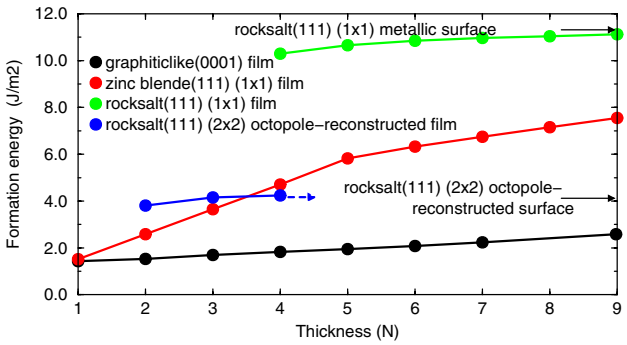

FIG. 1 (color online). Structural phase diagram for MgO(111) ultrathin films (from Ref. [9], Fig. 2, with extension to larger film thickness). Formation energy is given with respect to rocksalt bulk MgO; film thickness is defined as the number of formula units in the (1×1) unit cell.

The present study is based on the gradient-corrected [14] density-functional theory implemented in VASP [15]. The numerical setup is similar to that used in Ref. [9]. For MgO and NaCl we use ultrasoft pseudopotentials [16]. The projector-augmented wave (PAW) method [17] describes the electron-ion interaction in ZnO. A slab geometry, with a (1×1) two-dimensional (2D) unit cell, is adopted throughout the study, with corrections for the residual dipole. All atomic degrees of freedom are relaxed. Atomic charges are estimated within a Bader method [18]. The films are stoichiometric and unsupported, which approximates well the deposition on a weakly interacting substrate, such as the widely used silver surfaces [9]. The film thickness is defined as the number N of formula units in the unit cell. We define the structural parameter R as a ratio between the mean shortest distance between anion and cation planes R_1 and the mean distance between planes of the same chemical composition $R_1 + R_2$. We remind that R enters the electrostatic compensation criterion $R = \delta Q/Q$ which determines the surface charge excess δQ (with respect to the bulk value Q) necessary for stabilization of polar surfaces [2].

We first focus on zinc blende MgO films and replot their formation energy with respect to zinc blende MgO bulk: $E_{\text{form}} = E_{\text{film}} - NE^{\text{ZB}}_{\text{bulk}}$. In this way we eliminate any spurious linear contribution due to the difference of bulk RS and ZB energies $N(E^{\text{ZB}}_{\text{bulk}} - E^{\text{RS}}_{\text{bulk}})$ (such as those visible in Fig. 1 for the graphiticlike and zinc blende phases). Figures 2(a)–2(c) evidence a transition at a critical thickness $N_C \approx 4$–5 between a low- and a high-thickness regime. The formation energy varies linearly at low thickness: $E_{\text{form}} \approx E_0 + \alpha N$. Beyond N_C, the behavior changes qualitatively and the formation energy converges asymptotically towards the cleavage energy E_{cl}: $E_{\text{form}} \approx E_{\text{cl}} - \beta/N$. At low thickness, the lateral lattice parameter increases with N and then decreases for $N > N_C$. Except for $N = 1$, where it is strictly equal to zero, the structural parameter R is very small and quasi-independent of N. Both the increase of the lateral lattice parameter and the strong reduction of R are due to a considerable flattening of the bilayers (small R_1) with respect to bulk geometry, Fig. 2(b). This effect is also at the origin of a reduced total dipole moment. R suddenly increases at the transition and asymptotically converges to the bulk value. As long as $N < N_C$, the charge modification δQ (with respect to the bulk value Q) on the outer layers is practically negligible, while in the whole high-thickness regime, the asymptotic relationship $\delta Q/Q \approx R_1/(R_1 + R_2)$ is well obeyed. At low thickness, the dipole moment and the associated electrostatic potential $\Phi(N)$ grow linearly with N. In the high-thickness regime, their variation is very weak and $\Phi(N)$ converges rapidly towards a constant value Φ_{sat}. The gap between the valence (VB) and the conduction (CB) bands is open in the low-thickness regime and decreases quasilinearly with the number of oxide layers. It is closed when $N \geq 5$. Figure 2(d) displays the projected density of states of the oxygen $2s$ levels for films of different thicknesses $(1 \leq N \leq 7)$. For a given N, the $2s$ levels of oxygens in the successive layers are shifted with respect to one another. The total width of the $2s$ band increases progressively as long as $N < N_C$ and stays practically constant when N is larger than N_C.

The low-thickness films are thus *uncompensated* polar systems, characterized by an insulating electronic structure, negligible δQ, and in which the dipole moment and the formation energy grow linearly as a function of the film thickness. Except for $N = 1$, the films can thus be viewed as an association of identical capacitors, with constant charges $\pm Q$ per 2D unit cell, and uniform layer spacings. Such an image accounts for the linear increase of $\Phi(N)$ and

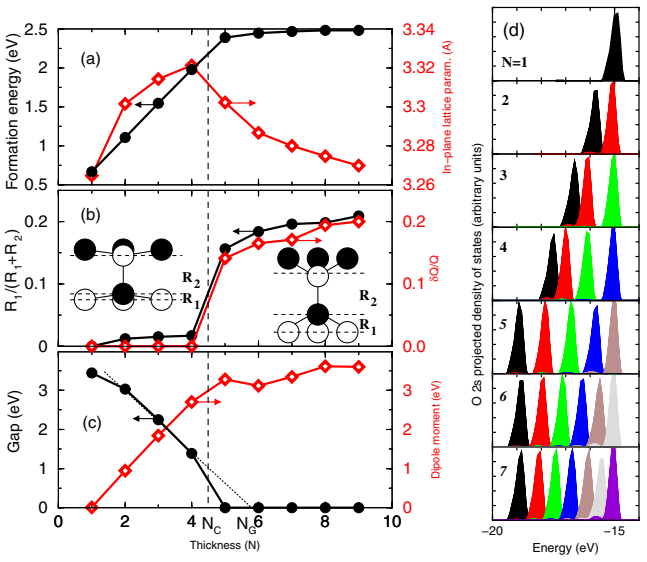

FIG. 2 (color online). MgO(111) fcc films: (a) in-plane lattice parameter and formation energy, (b) structural parameter $R_1/(R_1 + R_2)$ and relative surface charge $\delta Q/Q$, (c) gap G and dipole moment, (d) local density of states of oxygen $2s$ levels (the Fermi level is at $E_F = 0$), as a function of film thickness. Sketches of distorted (low-thickness) and bulklike (high-thickness) structures are given in the insets (b).

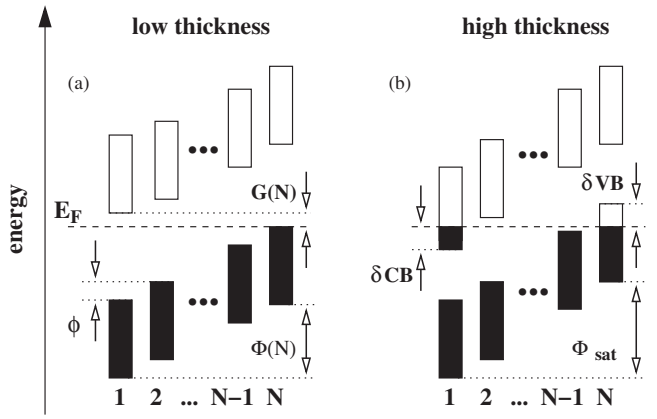

FIG. 3. Sketch of the electronic structure of ultra thin films in the low- and high-thickness regimes. First bilayer corresponds to the cation-terminated film surface.

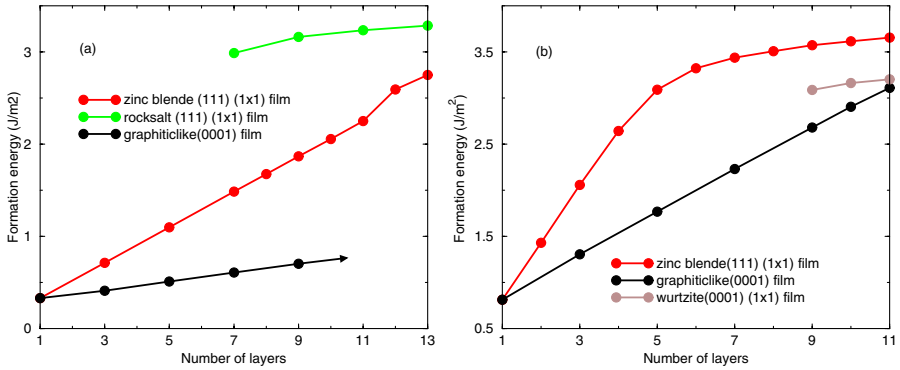

FIG. 4 (color online). Calculated structural phase diagram for (a) NaCl and (b) ZnO ultrathin (111) films. Corresponding formation energies are given with respect to rocksalt bulk NaCl and to wurtzite bulk ZnO, respectively.

E_{form} as a function of N. The electrostatic potential $\Phi(N)$ associated with the total dipole includes a contribution due to the nonvanishing R_1 plus an intrinsic contribution ϕ_0 due to the polarization of the electronic clouds in their asymmetric local environment. It is worth pointing out that contrary to the hexagonal graphiticlike stacking, ϕ_0 is nonzero also for perfectly flat ($R_1 = 0$) fcc films. $\Phi(N)$ reads (with A the 2D cell area):

$$\Phi(N) \approx (4\pi R_1 Q/A + \phi_0)N = \phi N, \qquad (1)$$

where ϕ denotes a mean increase of the electrostatic potential per bilayer, which, as depicted in Fig. 3(a), shifts the successive local bands, in agreement with the numerical results in Fig. 2(d). Neglecting the band dispersion and distortions (i.e., the possible band narrowing at the surface), the total gap $G(N)$ thus decreases roughly linearly with N, with a slope equal to $-\phi$. We define N_G as the film thickness at which it extrapolates to zero. In the case of MgO, Fig. 2(c), $N_G = 5$–6 is slightly larger than the critical thickness $N_C = 4$–5.

In the absence of charge modification, the formation energy in the low-thickness regime $E_{\text{form}} = E_0 + \alpha N$ includes an electrostatic term (dipole contribution) plus a strain contribution due to the structural deformation with respect to the bulk structure. A small $R_1/(R_1 + R_2)$ reduces the electrostatic contribution but costs elastic energy. The very small values of R_1 found in this study (roughly one tenth of the bulk one) show that the electrostatic term related to the film polarity is the driving force in this thickness regime.

In the high-thickness regime, the system switches to a geometry whose structural parameter R is reminiscent of the bulk zinc blende atomic structure. This regime is close to that described already in the literature for semi-infinite polar surfaces. The total gap is closed (metallic surface) and a charge redistribution δQ takes place on the outer layers of the film (filling δCB of the surface CB and depletion δVB of the surface VB), providing a compensation of the divergent dipole moment, Fig. 3(b). The local bands are shifted by the electrostatic potential due to (1) the cumulated dipole moment of the atomic layers, (2) the compensating dipole due to surface charges δQ, and (3) additional surface contributions due to intra-atomic interactions associated to the charge modification δQ. In this regime, the total electrostatic potential converges rapidly towards a constant value $\Phi_{\text{sat}} \neq 0$, consistently with the constant width of the $2s$ oxygen levels for $N \geq 5$ in Fig. 2(d). Alignment of the Fermi level E_{F} enables the

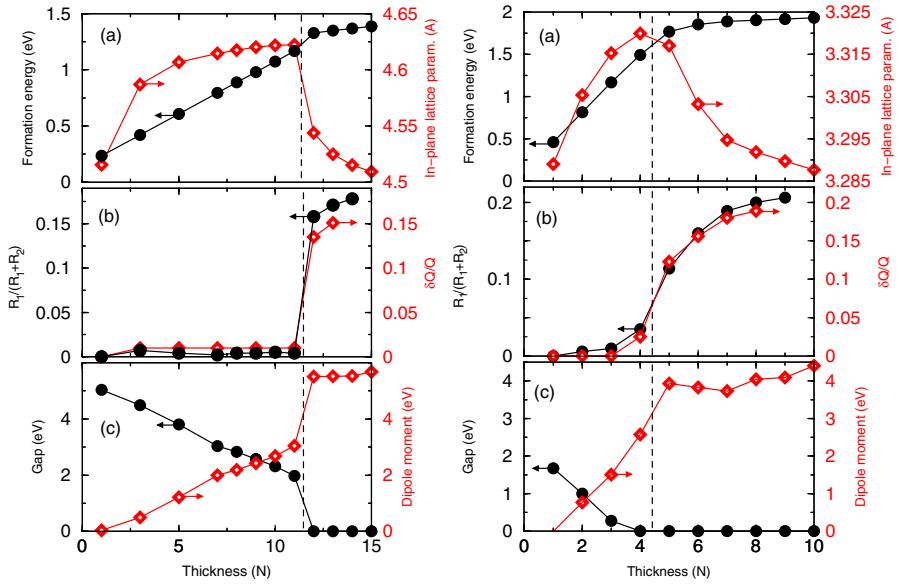

FIG. 5 (color online). NaCl (left) and ZnO (right) fcc films: (a) formation energy and the in-plane lattice parameter, (b) $R_1/R_1 + R_2$ and $\delta Q/Q$, (c) gap and dipole moment, as a function of film thickness. N_C is indicated with dashed lines.

TABLE I. Energetic, structural, and electronic characteristics of fcc (111) MgO, NaCl, and ZnO films (see text). All quantities refer to a (1×1) surface cell.

	E_{cl} (eV)	α (eV)	N_C	Q	ϕ (eV)	ϕ_0 (eV)	Φ_{sat} (eV)	N_G
MgO	2.5	0.45	4–5	1.70	0.9	0.3	3.6	5–6
NaCl	1.5	0.10	11–12	0.87	0.3	0.25	5.5	17–18
ZnO	2.0	0.33	4–5	1.22	0.75	0.3	4.5	3–4

determination of δQ in the form:

$$\delta Q = Q \frac{R_1}{(R_1 + R_2)} \frac{[1 + \eta - O(N^{-1})]}{[1 + O(N^{-1})]}. \quad (2)$$

As expected, in the limit $N \to \infty$, $\delta Q/Q$ converges towards $R_1/(R_1 + R_2)$, with a usually weak corrective term $\eta = \phi_0 A/4\pi Q R_1$ (of the order of 0.01 in MgO). The approach to the asymptotic limit is in $1/N$, due to the term in the numerator (in agreement with Ref. [19]). Derivation of Eq. (2) and discussion of the origin of the additional $1/N$ term in denominator will be given elsewhere [20].

We stress that although a closed electronic gap is a necessary condition for the existence of the charge modification akin to the high-thickness regime, the transition is driven solely by energetic considerations. Taking into account the intrinsically linear behavior of the formation energy in the low-thickness regime and its weak dependence on the slab thickness at high thicknesses, the transition thickness can qualitatively be deduced from $E_0 + \alpha N_C \approx E_{cl}$.

The scenario described above for MgO applies also to other compounds of the same (e.g., NaCl) or of a different (e.g., ZnO) bulk crystallographic structure. Both NaCl and ZnO, Fig. 4, display a low-thickness phase diagram similar to MgO, with graphiticlike(0001) and zinc blende(111) as the lowest energy phases. As regards polar zinc blende(111) films, Fig. 5, ZnO and NaCl present some specificities with respect to MgO. Indeed, while for ZnO, N_C is close to that in MgO, in NaCl the transition occurs at a much higher thickness, Table I. This can be assigned to the smaller NaCl valence, which makes the formation energy slope α about 4 times smaller than that of the oxides, conjugated to a value of the cleavage energy E_{cl} which is only twice smaller in NaCl. More interestingly, while for MgO and ZnO $N_G \sim N_C$, in NaCl the gap is far from being closed at the transition: $N_C < N_G$. The transition thus produces a discontinuity in structural and electronic characteristics, left panel of Fig. 5, reminiscent of a first order transition. The very slow gap decrease in NaCl films in the low-thickness regime is mostly due to the very small mean potential increase ϕ (close to the polarization term ϕ_0, Table I), which itself originates from the conjugated effect of weaker ionicity Q, larger surface area A, and a smaller R_1. In MgO, N_C is also smaller than N_G, but the difference $N_G - N_C$ is of the order of unity, so that the discontinuities are nearly invisible. On the other hand, ZnO exemplifies the case where N_C is slightly larger than N_G. In this case, an intermediate regime exists in which the electron redistribution proceeds progressively, rather than abruptly. As a function of film thickness, the structural and electronic characteristics, right panel of Fig. 5, display an S-shape behavior rather than a discontinuity.

In summary, we have used *ab initio* calculations to model ultrathin MgO, ZnO, and NaCl films of polar orientation. For the first time, we unravel the thickness-dependent behavior of polarity and demonstrate that there exists a peculiar, unexpected low-thickness regime, in which the film polarity is uncompensated. This regime corresponds to insulating polar stacking with strongly thickness-dependent properties (gap, dipole moment). Our present study gives a general theoretical background to polarity in ultrathin films and a well founded guideline to stimulate experimental characterization and fabrication of polar nanostructures, with unusual physical and chemical properties.

We are grateful to J. Jupille, N. Jedrecy, F. Finocchi, G. Pacchioni, and C. Henry for fruitful discussions. This work was supported by the COST actions No. D-19 and No. D-41.

[1] P. W. Tasker, J. Phys. C **12**, 4977 (1979).
[2] C. Noguera, J. Phys. Condens. Matter **12**, R367 (2000).
[3] G. A. Rizzi *et al.*, Surf. Sci. **482–485**, 1474 (2001).
[4] M. Kiguchi *et al.*, Phys. Rev. B **68**, 115402 (2003); R. Arita *et al.*, Phys. Rev. B **69**, 235423 (2004).
[5] W. Ranke, M. Ritter, and W. Weiss, Phys. Rev. B **60**, 1527 (1999); E. D. L. Rienks, N. Nilius, H. P. Rust, and H. J. Freund, Phys. Rev. B **71**, 241404(R) (2005).
[6] S. Entani, M. Kiguchi, and K. Saiki, Surf. Sci. **566–568**, 165 (2004); R. Shantyr, C. Hagendorf, and H. Neddermeyer, Thin Solid Films **464–465**, 65 (2004).
[7] W. Hebenstreit, M. Schmid, J. Redinger, R. Podloucky, and P. Varga, Phys. Rev. Lett. **85**, 5376 (2000).
[8] F. Claeyssens *et al.*, J. Mater. Chem. **15**, 139 (2005).
[9] J. Goniakowski, C. Noguera, and L. Giordano, Phys. Rev. Lett. **93**, 215702 (2004).
[10] F. Finocchi *et al.*, Phys. Rev. Lett. **92**, 136101 (2004).
[11] C. L. Freeman *et al.*, Phys. Rev. Lett. **96**, 066102 (2006).
[12] N. Nilius *et al.*, Phys. Rev. Lett. **95**, 066101 (2005).
[13] S. K. Shaikhutdinov *et al.*, Phys. Rev. Lett. **91**, 076102 (2003).
[14] J. P. Perdew and Y. Wang, Phys. Rev. B **45**, 13 244 (1992).
[15] G. Kresse and J. Hafner, Phys. Rev. B **47**, 558 (1993); G. Kresse and J. Furthmüller, Phys. Rev. B **54**, 11 169 (1996).
[16] D. Vanderbilt, Phys. Rev. B **41**, 7892 (1990).
[17] P. E. Blöchl, Phys. Rev. B **50**, 17 953 (1994); G. Kresse and D. Joubert, Phys. Rev. B **59**, 1758 (1999).
[18] R. F. W. Bader, Chem. Rev. **91**, 893 (1991), implemented in ABINIT by K. Casek, F. Finocchi, and X. Gonze.
[19] G. Kresse, O. Dulub, and U. Diebold, Phys. Rev. B **68**, 245409 (2003); A. Eichler and G. Kresse, Phys. Rev. B **69**, 045402 (2004).
[20] C. Noguera and J. Goniakowski (unpublished).